Investigation of Structural Parameter Effects On Performance of Mach-Zehnder Interferometer

Negin Memar[1*]

[*]memar.negin@gmail.com

Abstract: The Mach-Zehnder interferometer (MZI) is a device used to determine the relative phase shift variations between two beams caused by a single source. MZIs in both TE and TM modes were designed, fabricated, measured, and characterized. Strip waveguides with a foundry standard thickness of 220 nm were used to design the MZIs. Transmission spectra, effective index, and group index for the silicon-based MZIs were simulated. Additionally, the effects of various parameters were investigated, including polarization, the impact of varying path lengths on the Free Spectral Range (FSR), and the influence of waveguide widths on the group index.

1. Introduction

In the last decades, integrated photonics has significantly contributed for the evolution of the optical communications industry. Namely, silicon photonics devices have shown high speed integration capabilities, associated with improved performance and reduced loss and power consumption. These features have been characterizing silicon photonics as a key element to support the capacity-bandwidth demand of the optical networks.

Silicon-based Mach-Zehnder Interferometer (MZI) is one of the main building-blocks in silicon photonic integrated circuits (PIC). It has attracted much attention and found applications in optical modulators, optical switching and optical routing. In this report, multiple MZI structures are investigated. At first, the conventional MZI with waveguide with cross section of 500×220 nm^2 is investigated for both the fundamental quasi-TE and quasi-TM modes considering waveguides in the strip configuration. Then, the same simulations are repeated for other MZIs with different path lengths in TE-mode. Additionally, simulations have been done for MZIs with different waveguide widths in TM-mode. By examination of the results, we can infer the overall effects of different path lengths, waveguide widths, and polarizations on the performance of the MZI to design the most suitable structure for our targeted application.

This work is devoted to the design, layout, and fabrication of Mach-Zehnder Interferometer (MZI) devices using silicon-on-insulator (SOI) wafers with strip waveguides. Figure 1 illustrates the cross-section of a typical SOI strip waveguide, which consists of four layers: the silicon substrate, buried oxide (BOX), the silicon waveguide core, and the oxide cladding. The strip-waveguide configuration is ideal for routing purposes and tight bends; furthermore, its fabrication process can achieve low propagation losses of 2–3 dB/cm.

This report is organized as follows: Section 2 briefly presents the interferometric principle that rules the MZI transfer function. Section 3 shows the model and the corresponding simulation results of the MZIs using Lumerical. Section 4 presents the layout mask for future fabrication and automated testing processes.

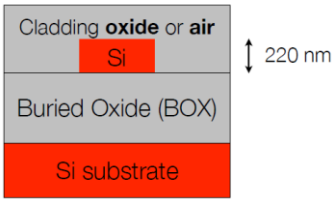

Fig. 1. Cross-section of a SOI wafer for strip waveguide

2. Theory of Mach Zehnder Interferometer (MZI)

A balanced MZI can be model as a 2-port device, formed by a beam-splitter at the input side and a beam-combiner at the output side, connected by waveguides with identical geometries and material properties. With this configuration, for any wavelength, the signals of the two arms of the MZI are constructively combined, in the MZI output (Figure 2).

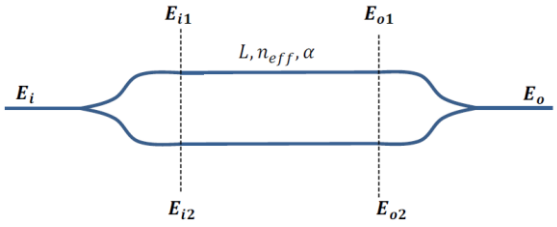

Fig. 2. Balanced MZI: Both arms have the same length L, effective index n_{eff}, and propagation loss α.

To exploit the different levels of interference, a length asymmetry can be included between the arms, as it is indicated in Figure 3. Besides, the two waveguides can present differences in their effective indexes (n_{eff1}, n_{eff2}) and attenuation constants (α_1, α_2). Thus, depending on the signal wavelength, the phase-mismatch between the two combined signals (E_{o1} *and* E_{o2}) causes different kinds of interference, from constructive to destructive.

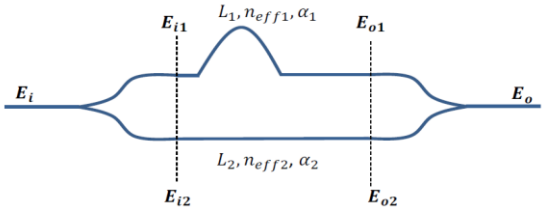

Fig. 3. Unbalanced MZI. Upper and lower arms have distinct properties.

The vectorial electrical field at the input of the MZI is represented by E_i. At the output of the beam-splitter, the complex electrical fields at the upper and lower arms are given by:

$$E_{i1} = E_{i2} = \frac{E_i}{\sqrt{2}}$$

The electrical fields at the input of the beam-combiner can be described by:

$$E_{o1} = E_{i1}.e^{-j\beta_1 L_1 - \frac{\alpha_1}{2}L_1}\ ,\quad E_{o2} = E_{i2}.e^{-j\beta_2 L_2 - \frac{\alpha_2}{2}L_2}$$

Where $\beta_{1,2}$ = ($2\pi/\lambda$) $n_{eff1,2}$ accounts for the propagation constants of the upper/lower arms. For the beam-combiner, each input field has the amplitude equally divided between the fundamental mode and the radiation modes. Thus,

$$E_o = \frac{1}{\sqrt{2}}(E_{o1} + E_{o2}) = \frac{1}{2}\left(E_{i1}.e^{-j\beta_1 L_1 - \frac{\alpha_1}{2}L_1} + E_{i2}.e^{-j\beta_2 L_2 - \frac{\alpha_2}{2}L_2}\right)$$

As the light intensity is proportional to the squared power of the field amplitude, the light intensity in the output of the MZI is:

$$I_o = \frac{1}{4}I_i\ |\left(E_{i1}.e^{-j\beta_1 L_1 - \frac{\alpha_1}{2}L_1} + E_{i2}.e^{-j\beta_2 L_2 - \frac{\alpha_2}{2}L_2}\right)|^2$$

The above equation represents the general form of an unbalanced MZI transfer function and output intensity. However, for the purpose of this work, we can neglect the loss relative to the constants α_1 and α_2. Besides, the propagation constants may also be considered equal ($\beta_1 = \beta_2 = \beta$) in both arms. Therefore, the equation can be simplified to:

$$I_o = \frac{1}{2}I_i\left(1 + Cos(\beta.\Delta L)\right)$$

Where $\Delta L = L_1 - L_2$, $\beta = \frac{2\pi n}{\lambda}$. Since β changes as a function of wavelength, we will get sinusoidal variations versus wavelength. The period of the oscillation is dependent on ΔL and on the waveguide properties.

The period between the peaks of the MZI transfer function, *i.e.*, the free spectral range (FSR), is calculated by:

$$FSR\ [nm] = \frac{\lambda^2}{\Delta L\ .n_g(\lambda)}\ ,\qquad FSR\ [GHz] = \frac{c}{\Delta L\ .n_g}$$

Where n_g is the group index, defined by:

$$n_g(\lambda) = n_{eff}(\lambda) - \lambda\frac{dn_{eff}(\lambda)}{d\lambda}$$

3. Modeling and Simulation

Lumerical MODE and INTERCONNECT were used for mode analysis and circuit simulation, respectively. To find the three coefficients of the waveguide compact model (based on Taylor expansion), a script in the Lumerical MODE was used.

3.1 Waveguide Modelling in Lumerical Mode

MODE simulation is done to find the spatial field distribution of TE and TM modes for different waveguide cross-sections. Mode profiles for four cross-sections (400×220, 500×220, 600×220 and 800×220 nm^2) at 1.5 μm wavelength are shown in Table 1 and 2 for TE and TM modes, respectively.

As the waveguide width increases (from 400 nm to 800 nm), the fundamental TE-mode becomes more tightly confined within the silicon core. This is visible in the heat maps, where the mode "spot" stays centered and fits more comfortably within the larger geometric boundaries. Besides, table 1 shows that the effective index of the fundamental mode (Mode #1) increases with width.

Unlike the TE-mode, the Fundamental TM-mode intensity is concentrated at the upper and lower horizontal interfaces of the silicon core. This is characteristic of TM modes in thin SOI waveguides, where the electric field is primarily perpendicular to the substrate. Moreover, the effective index of the fundamental mode increases as the waveguide widens

Table 1. TE-mode profiles for four different cross-sections at 1.5 μm.

	Fundamental TE-mode	Index
400 × 220	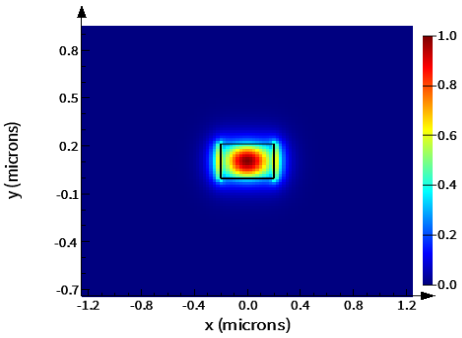	

mode #	effective index	wavelength (μm)	loss (dB/cm)	group index	TE polarization fraction (Ex)
1	2.298427+1.319796e-09i	1.5	0.00048019	4.402917+3.029140e-09i	97
2	1.749900+8.610531e-10i	1.5	0.00031328	3.728516+4.948361e-09i	5
3	1.436169+2.973687e-10i	1.5	0.00010819	1.851332+8.409343e-10i	51

500 × 220	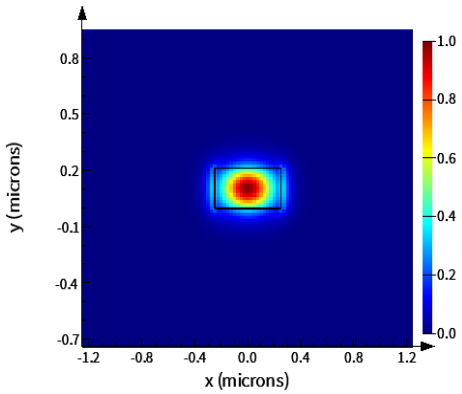	

mode #	effective index	wavelength (μm)	loss (dB/cm)	group index	TE polarization fraction (Ex)
1	2.503380+1.297784e-09i	1.5	0.00047218	4.196678+2.802685e-09i	99
2	1.836526+9.718270e-10i	1.5	0.00035358	4.007656+4.785887e-09i	4
3	1.532900+6.249787e-10i	1.5	0.00022739	2.815674+5.056740e-09i	70

600 × 220	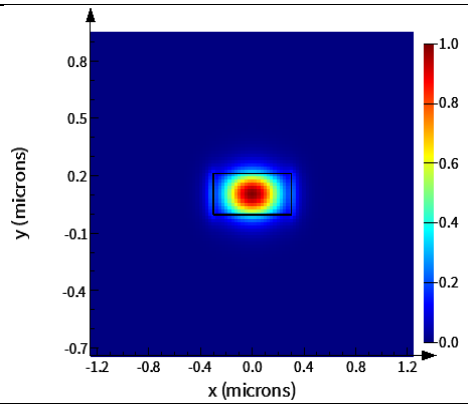	

mode #	effective index	wavelength (μm)	loss (dB/cm)	group index	TE polarization fraction (Ex)
1	2.616741+1.271579e-09i	1.5	0.00046264	4.061721+2.763219e-09i	99
2	1.899031+1.027928e-09i	1.5	0.00037399	4.129334+4.545809e-09i	4
3	1.778996+1.259895e-09i	1.5	0.00045839	4.511571+6.213950e-09i	88

800 × 220	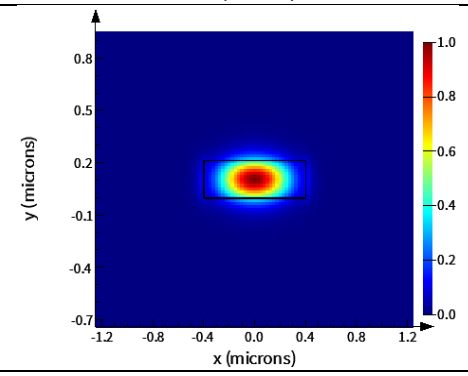	

mode #	effective index	wavelength (μm)	loss (dB/cm)	group index	TE polarization fraction (Ex)
1	2.730194+1.238813e-09i	1.5	0.00045072	3.921045+2.752779e-09i	100
2	2.249621+1.409665e-09i	1.5	0.00051288	4.588104+2.867610e-09i	98
3	1.977028+1.072256e-09i	1.5	0.00039012	4.200783+4.217023e-09i	3

Table 2. TM-mode profiles for four different cross-sections at 1.5 µm.

	Fundamental TM-mode	Index
400 × 220	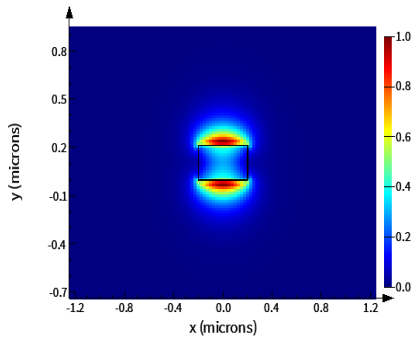	

mode #	effective index	wavelength (µm)	loss (dB/cm)	group index	TE polarization fraction (Ex)
1	2.298427+1.319796e-09i	1.5	0.00048019	4.402917+3.029140e-09i	97
2	1.749900+8.610531e-10i	1.5	0.00031328	3.728516+4.948361e-09i	5
3	1.436169+2.973686e-10i	1.5	0.00010819	1.851332+8.409351e-10i	51

500 × 220	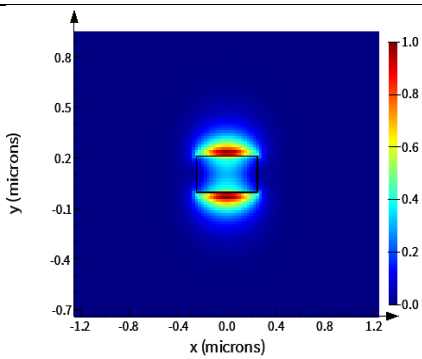	

mode #	effective index	wavelength (µm)	loss (dB/cm)	group index	TE polarization fraction (Ex)
1	2.503380+1.297784e-09i	1.5	0.00047218	4.196678+2.802685e-09i	99
2	1.836526+9.718270e-10i	1.5	0.00035358	4.007656+4.785887e-09i	4
3	1.532900+6.249787e-10i	1.5	0.00022739	2.815674+5.056740e-09i	70

600 × 220	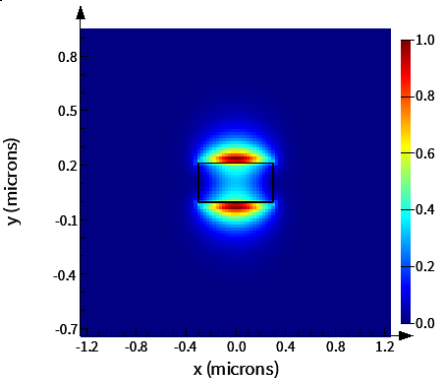	

mode #	effective index	wavelength (µm)	loss (dB/cm)	group index	TE polarization fraction (Ex)
1	2.616741+1.271579e-09i	1.5	0.00046264	4.061721+2.763219e-09i	99
2	1.899031+1.027928e-09i	1.5	0.00037399	4.129334+4.545809e-09i	4
3	1.778996+1.259895e-09i	1.5	0.00045839	4.511571+6.213950e-09i	88

800 × 220	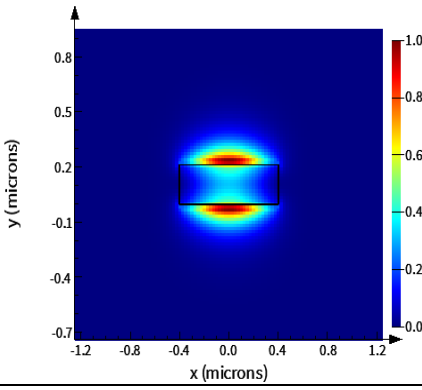	

mode #	effective index	wavelength (µm)	loss (dB/cm)	group index	TE polarization fraction (Ex)
1	2.730194+1.238813e-09i	1.5	0.00045072	3.921045+2.752779e-09i	100
2	2.249621+1.409665e-09i	1.5	0.00051288	4.588104+2.867610e-09i	98
3	1.977028+1.072256e-09i	1.5	0.00039012	4.200783+4.217023e-09i	3

The effective index and group index of both TE and TM modes versus wavelength are shown in table 3, table 4, table 5 and table 6 for different waveguide widths (400, 500, 600 and 800 nm). The effective index is decreasing with wavelength, and the group index is increasing with wavelength.

Table 3. Effective index and group index of the fundamental TE and TM modes verses wavelength for 400×220 nm^2

	Fundamental TE-mode	Fundamental TM-mode
n_{eff}	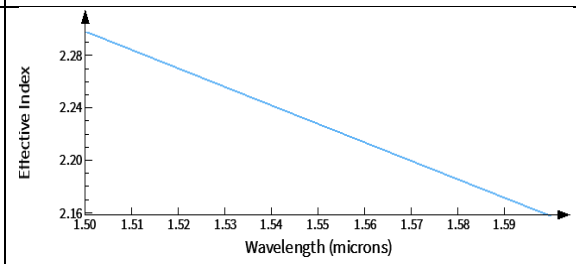	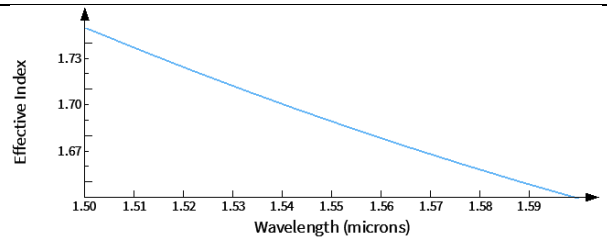
n_g	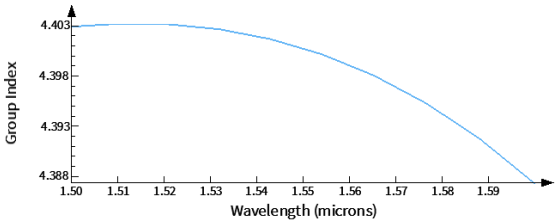	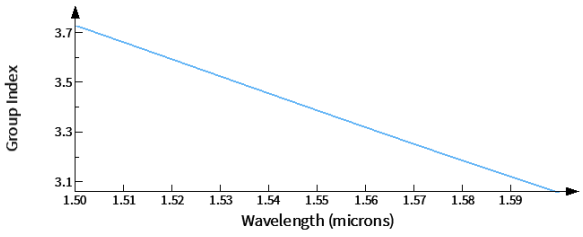

Table 4. Effective index and group index of the fundamental TE and TM modes verses wavelength for 500×220 nm^2

	Fundamental TE-mode	Fundamental TM-mode
n_{eff}	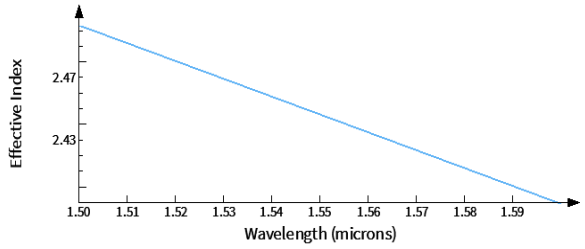	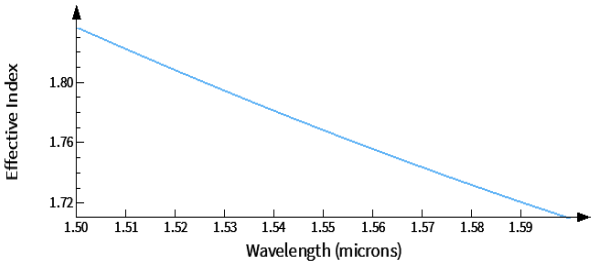

n_g	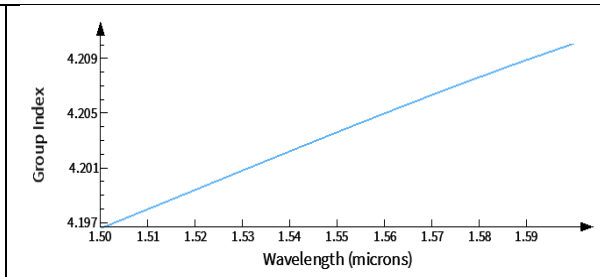	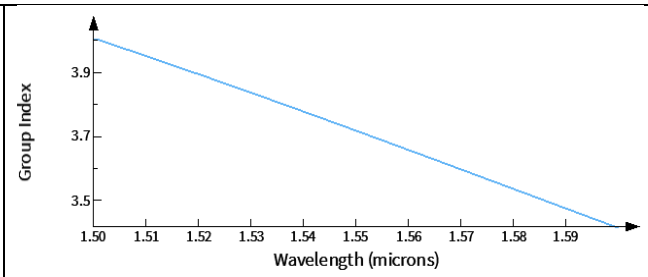

Table 5. Effective index and group index of the fundamental TE and TM modes verses wavelength for 600×220 nm^2

	Fundamental TE-mode	Fundamental TM-mode
n_{eff}	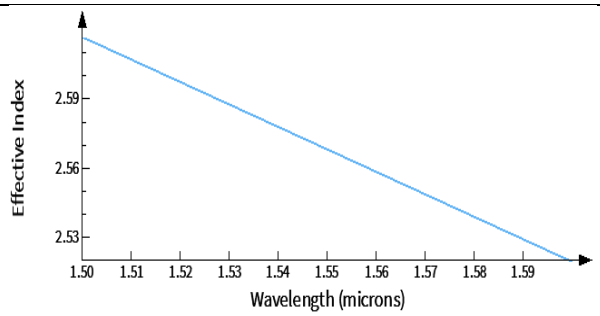	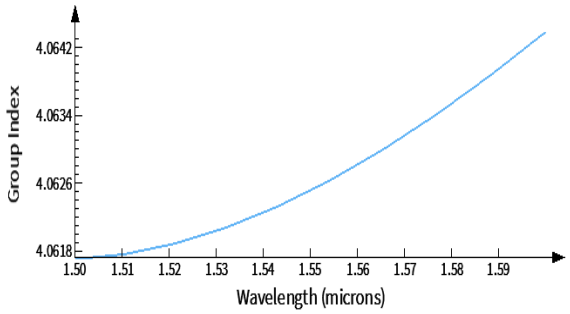
n_g	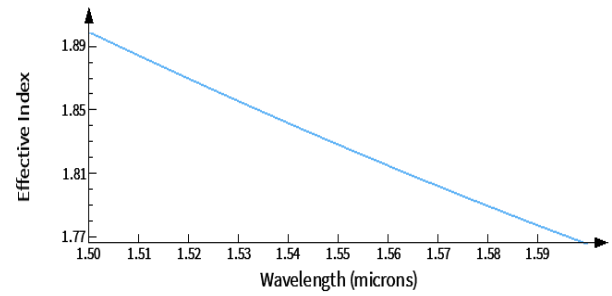	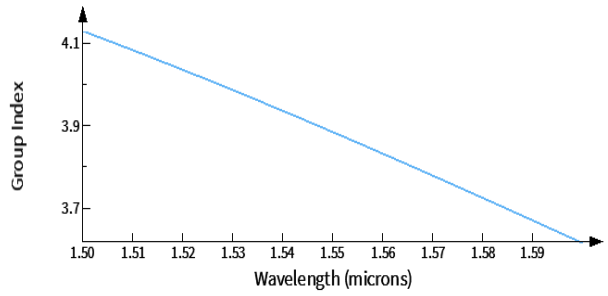

Table 6. Effective index and group index of the fundamental TE and TM modes verses wavelength for 800×220 nm^2

	Fundamental TE-mode	Fundamental TM-mode
n_{eff}	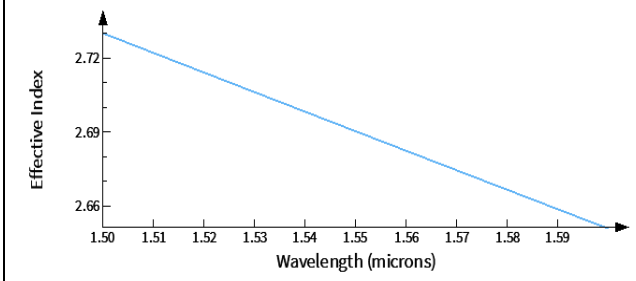	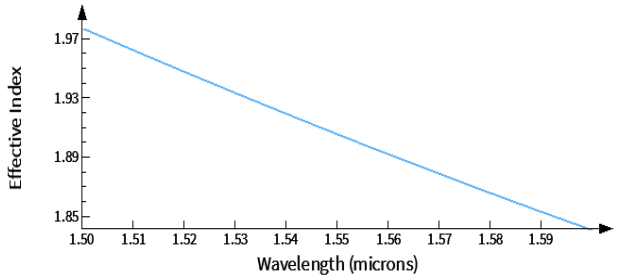
n_g	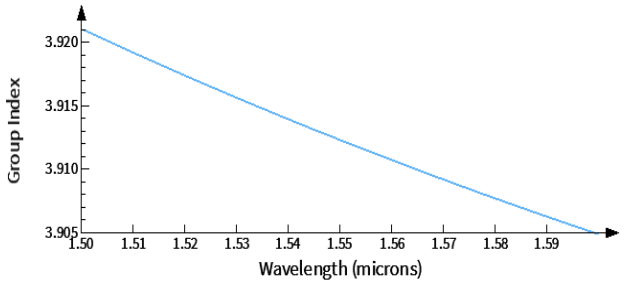	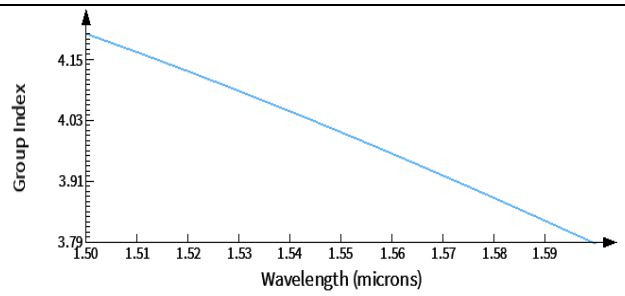

3.2 Waveguide Compact Model

Using the data exported from frequency sweep, the three coefficients of the Taylor expansion for compact model are found for all waveguide geometries and for both polarizations using a script in Lumerical MODE. The Taylor expansion is:

$$n_{eff,TE}(\lambda) = n_1 + n_2(\lambda - \lambda_0) + n_3(\lambda - \lambda_0)^2$$

$$n_{eff,TM}(\lambda) = n_1 + n_2(\lambda - \lambda_0) + n_3(\lambda - \lambda_0)^2$$

The Taylor expansion parameters can also be converted to conventional parameters (effective index, group index, and dispersion) at the wavelength λ_0:

$$n_{eff} = n_1$$
$$n_g = n_1 - n_2\,\lambda_0$$

$$D = -2\,\lambda_0 \frac{n_3}{c}\ [s/m^2]$$

The coefficients n_1, n_2, and n_3 are listed in table 7 for all waveguides and polarizations at $\lambda_0 = 1.5$ µm.

Table 7. Taylor expansion coefficients for different waveguides (**λ_0=1.55 µm**)

Cross section	Fundamental quasi-TE	Fundamental quasi-TM
400×220	$n_1 = 2.22829$ $n_2 = -1.40236$ $n_3 = 0.0845582$ 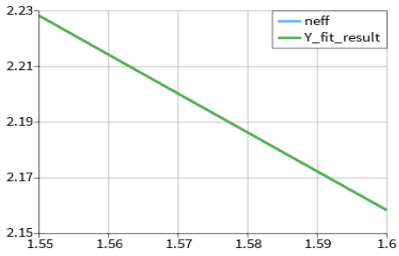	$n_1 = 1.68953$ $n_2 = -1.09461$ $n_3 = 2.08537$ 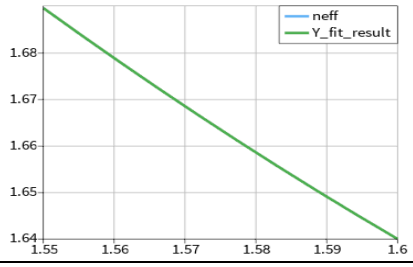
500×220	$n_1 = 2.44682$ $n_2 = -1.13352$ $n_3 = -0.041065$ 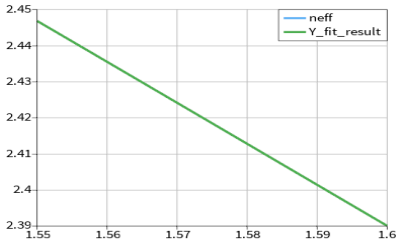	$n_1 = 1.76882$ $n_2 = -1.25896$ $n_3 = 1.92378$ 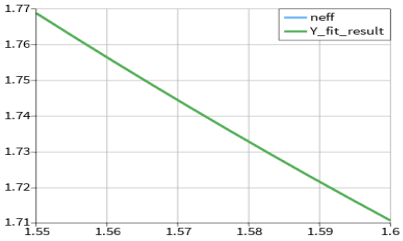
600×220	$n_1 = 2.56856$ $n_2 = -0.963796$ $n_3 = -0.0118806$ 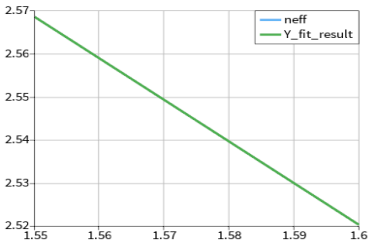	$n_1 = 1.82861$ $n_2 = -1.3282$ $n_3 = 1.70037$ 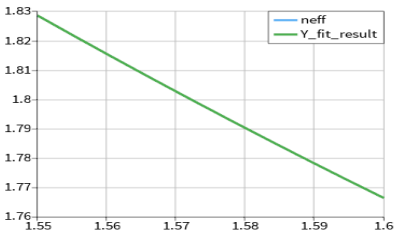
800×220	$n_1 = 2.69065$ $n_2 = -0.788107$ $n_3 = 0.0468452$ 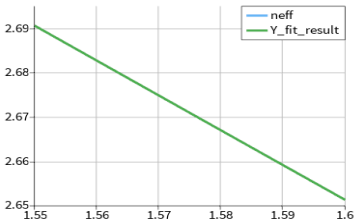	$n_1 = 1.906$ $n_2 = -1.35716$ $n_3 = 1.38996$ 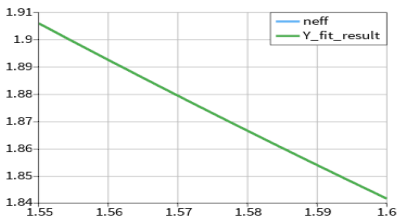

3.3 Waveguide Temperature Dependence

We simulated the temperature dependence of an optical waveguide. The silicon thermo-optic coefficient is $\frac{dn}{dT} = 1.86 \times 10^{-4}\, K^{-1}$. We wish to find the change in the waveguide effective index versus temperature $\frac{dn_{eff}}{dT}$. We wanted to see the effect of 10 degrees change in the temperature.

```
> ?getdata('FDE::data::mode1','neff');
result:
2.22248+6.89751e-11i
> ?neff_0=abs(getdata('FDE::data::mode1','neff'));
result:
2.22248
> ?neff_10=abs(getdata('FDE::data::mode1','neff'));
result:
2.22444
> ?(neff_10 - neff_0)/10;
result:
0.000196125
```

Therefore, the thermos-optic coefficient for a silicon waveguide is 0.000196125.

3.4 Y-Branch Simulations using Lumerical MODE 2.5D FDTD

Figure 4 shows the Y-branch simulated in Lumerical MODE.

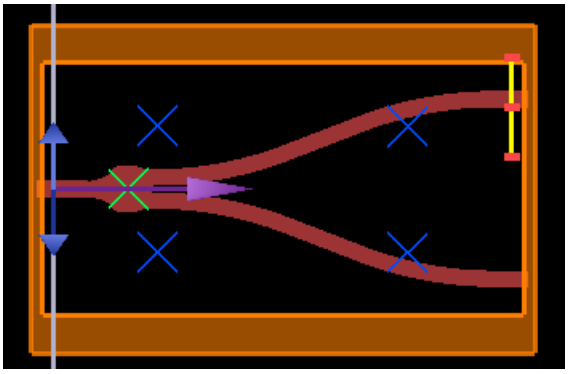

Fig. 4: Y-branch in Lumerical MODE

Figure 5 shows the transmission (T) of the Y-branch versus wavelength.

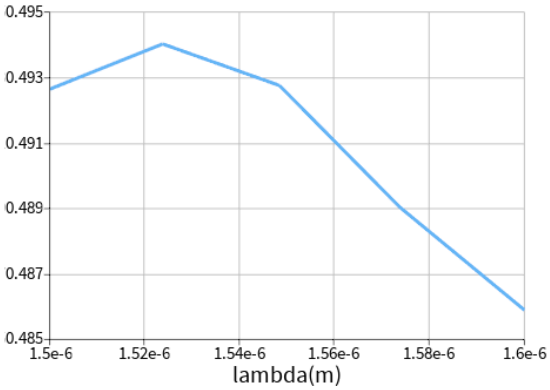

Figure 5: Y-branch transmission spectrum

3.5 Waveguide Bends Simulation using Lumerical MODE

Light propagating in a bend gets pushed out to the side. This will lead to two additional types of losses, mode mismatch losses and radiation losses. Mode mismatch is the dominant source of loss. Radiation loss is very small in strip waveguides. However, it does play a role in rib waveguides.

For the TE-mode and 5 μm bend, the power coupling was 0.99864 which is about 0.14% loss. The optimization finds that a shift of 10 nm would change the power coupling to 0.99949 which is about 0.05% loss, nearly 3 factor of improvement.

For the TM mode and 5 μm bend, the power coupling is 0.92269 which is about 7.7% loss. Optimizing the position shows that a 60 nm offset changes the power coupling to 0.943371 and reduces loss to about 5.6%. The TM-mode is more strongly affected by the bend compared to the TE-mode. For the 10 μm bend, the power coupling is 0.978797 and the loss is 3%.

3.6 Lumerical Interconnect

We provided the S-parameter file to the INTERCONNECT and plotted the insertion loss of the Y-branch as shown in figure 6.

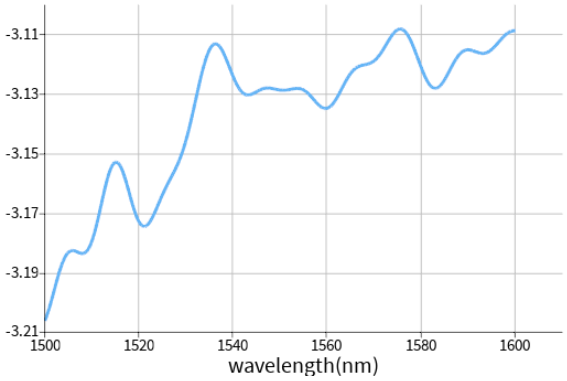

Figure 6: IL vs. wavelength for the Y-branch

Next, we characterize the MZI using 2 Y-branches and 2 waveguides. Figure 7 shows the MZI circuit in INTERCONNECT. Note that there is a 100 µm length difference between the two arms of the MZI.

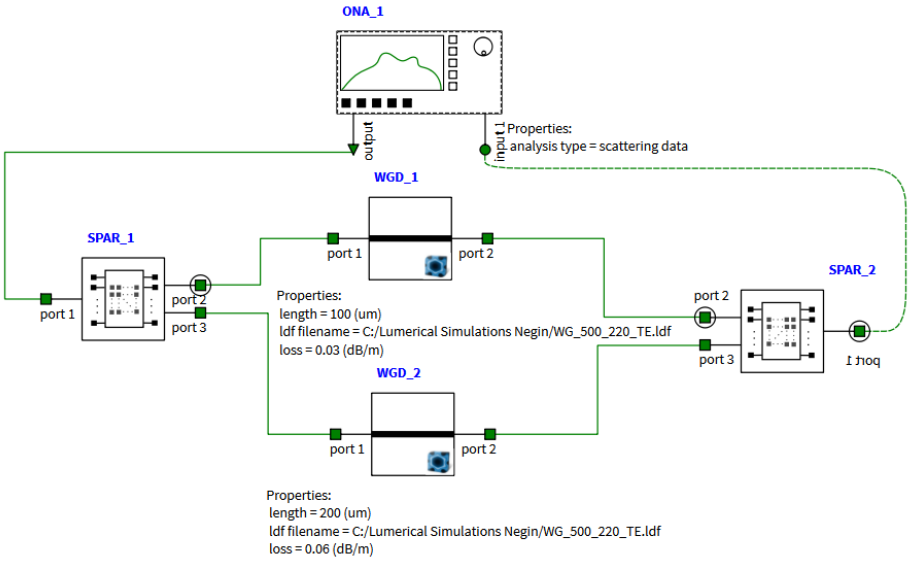

Figure 7: MZI in INTERCONNECT

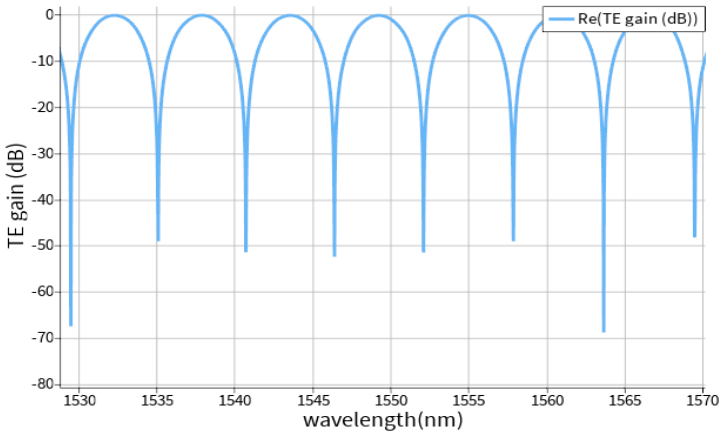

Figure 8: MZI TE gain in dB vs. wavelength

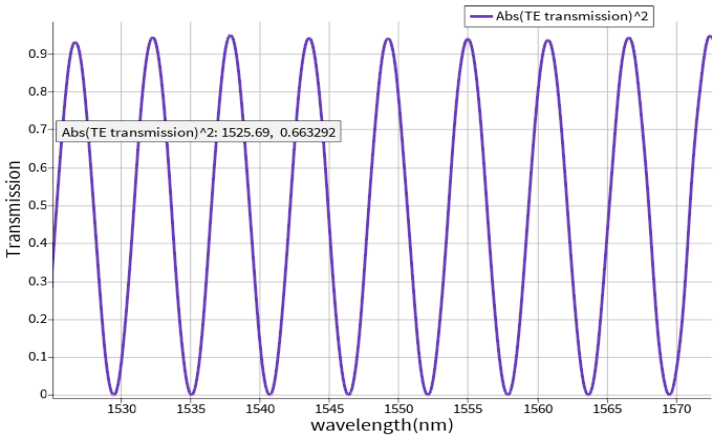

Figure 9: MZI TE transmission vs. wavelength

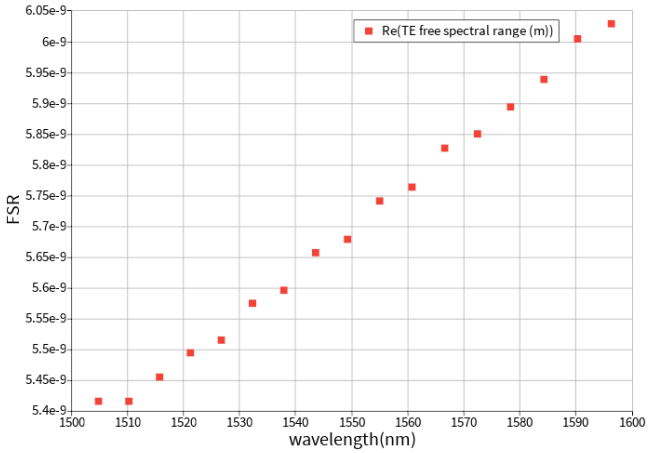

Figure 10: MZI FSR vs. wavelength

We used the script prompt to find the FSR:

```
> ?1550e-9^2/100e-6/4.2;
result:
5.72024e-09
> ?getresultdata('ONA_1', 'input 1/mode 1/peak/free spectral range');
result:
6.02855e-09
6.0041e-09
5.93817e-09
5.89382e-09
5.84997e-09
5.8269e-09
5.76356e-09
5.74115e-09
5.67906e-09
5.65728e-09
5.5964e-09
5.57524e-09
5.51553e-09
5.49496e-09
5.45541e-09
```

Next, we compare the transmission of the two MZI, one with 100 µm and the other with a 200 µm path difference between the arms. The FSR is two times smaller for the 200 µm mismatch as shown in figure 11.

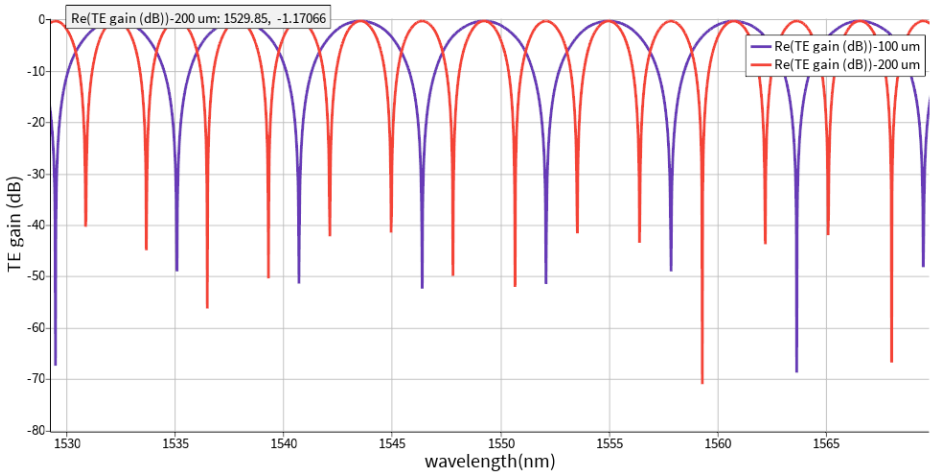

Fig. 11: TE gain in dB vs. wavelength for two MZI with 100 µm and 200 µm mismatch

Next, we add the fibre grating coupler to the MZI circuit. Figure 12 shows the circuit in INTERCONNECT.

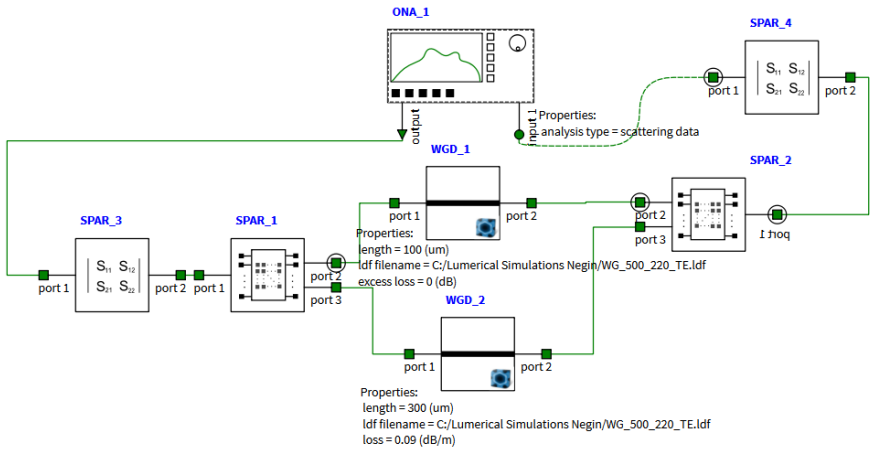

Fig. 12: MZI with grating couplers in INTERCONNECT

At 1550, the insertion of the circuit without grating couplers is about 0.3 dB. Whereas, with the two grating couplers, it is over 5 dB (Fig. 13).

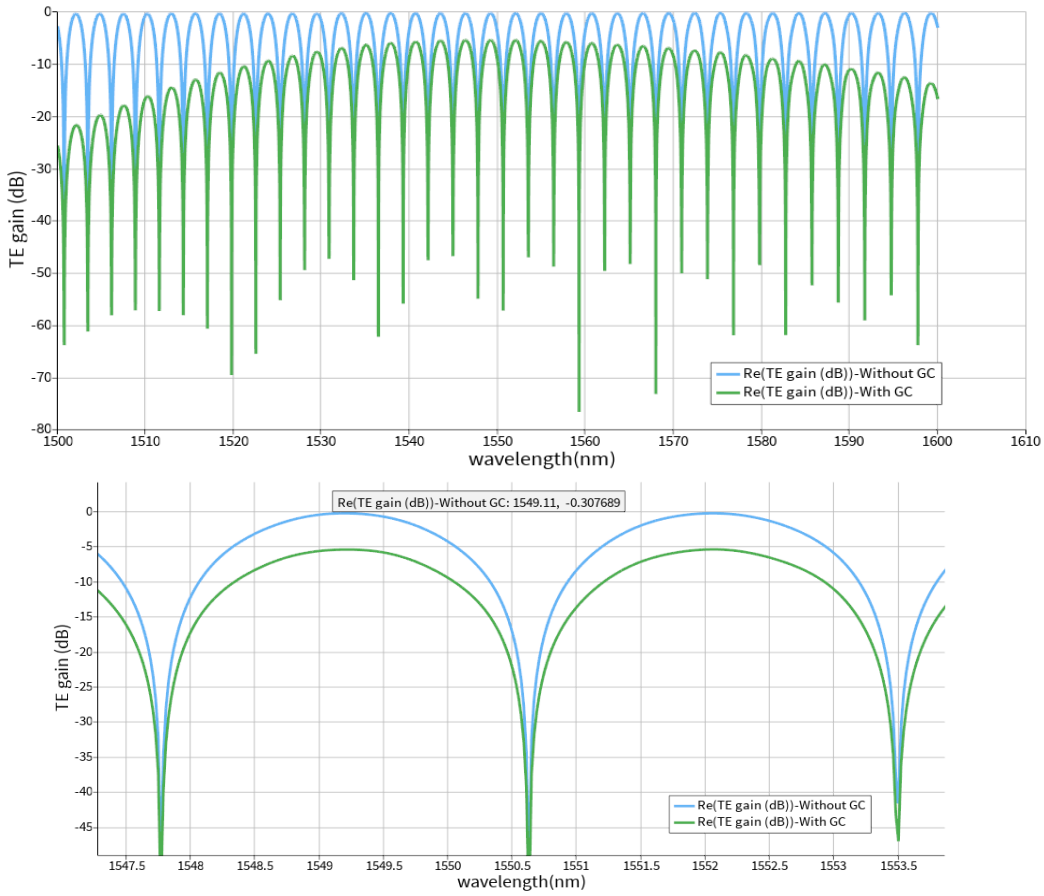

Fig. 13: MZI with and without grating couplers

The best-case insertion loss for the one and two grating couplers was simulated and found to be 2.55 dB and 5.06 dB, respectively. The grating coupler's transfer function, depicted in Figure 17, shows insertion losses ranging from 2.55 dB to 11 dB.

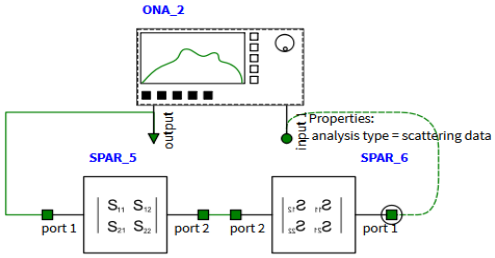

Fig. 14: Two grating couplers connected to a network analyzer.

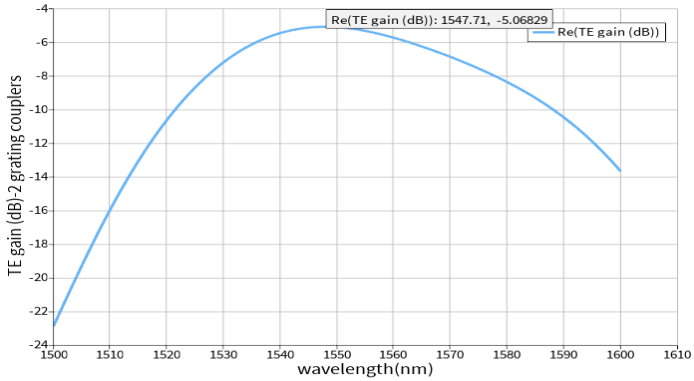

Fig. 15: Transmission of two grating couplers connected to a network analyzer.

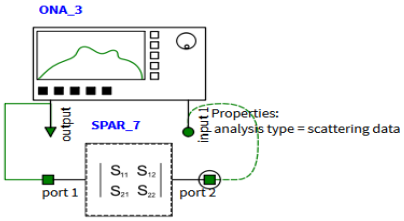

Fig. 16: One grating coupler connected to a network analyzer.

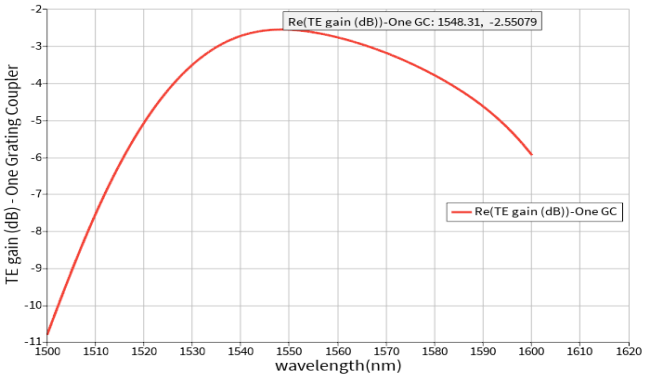

Fig. 17: Transmission of one grating coupler connected to a network analyzer.

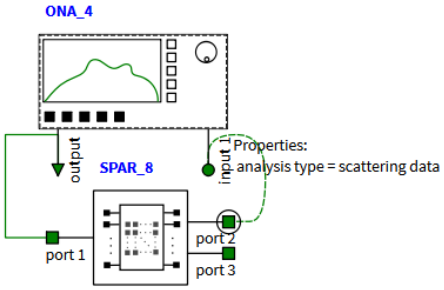

Fig. 18: One Y-branch connected to a network analyzer.

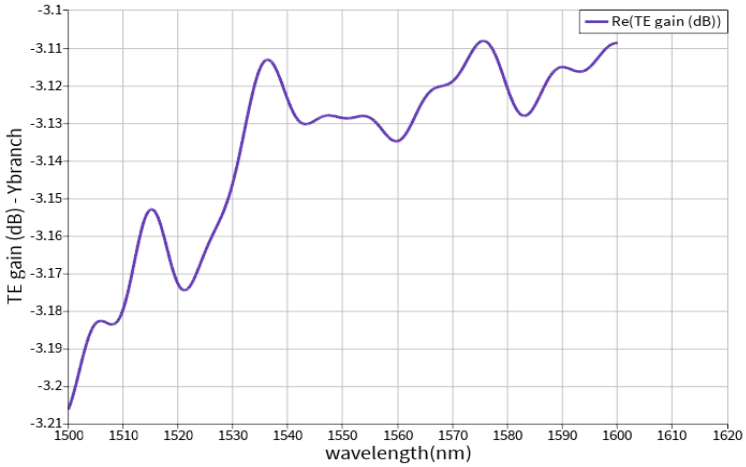

Fig. 19: Transmission of one Y-branch connected to a network analyzer.

3.7 Building Interferometer circuits using the Compact Model Library

In this section, we simulate a MZI using the Ebeam compact model library.

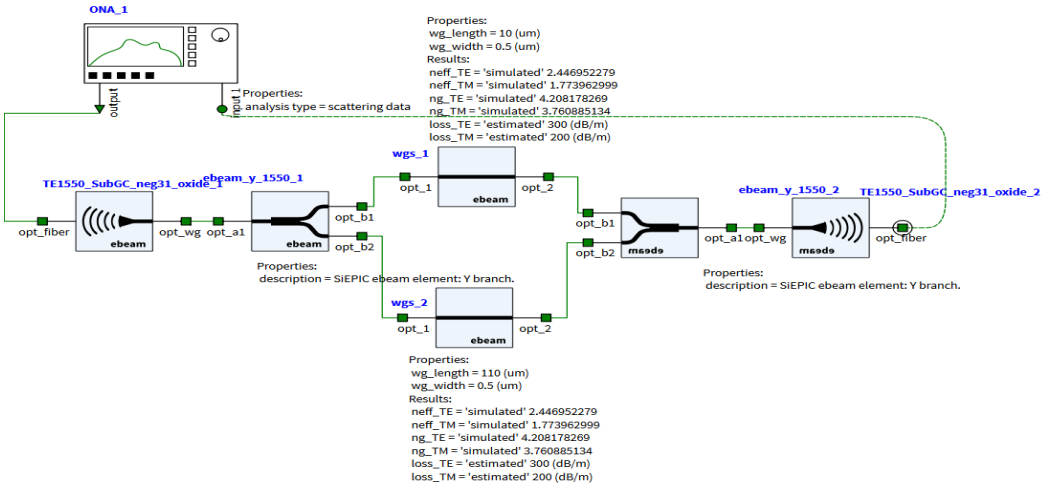

Fig. 20: MZI with Y-branches in INTERCONNECT

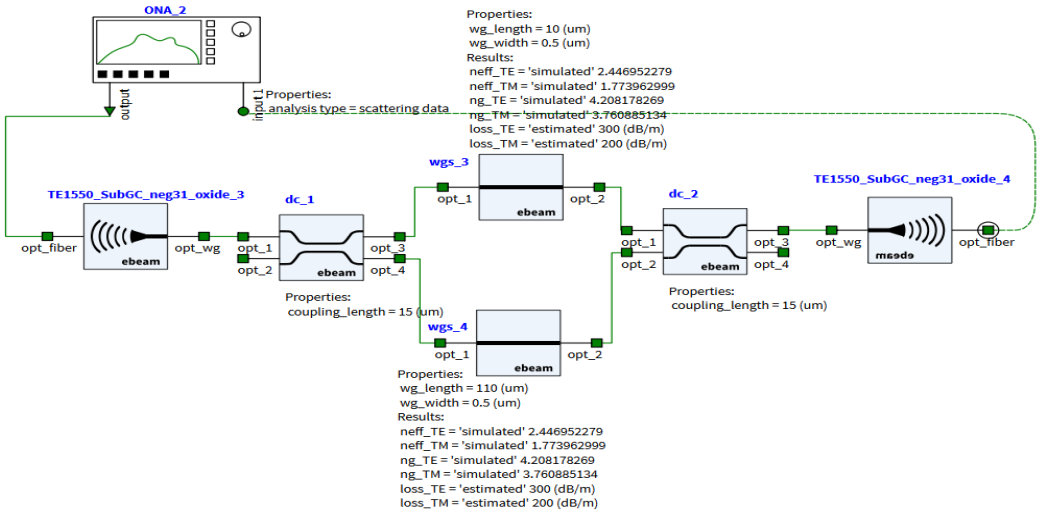

Fig. 20: MZI with directional couplers in INTERCONNECT

The extinction ratio using the directional couplers is not as large as with the Y-branch. There is a wavelength dependance to the extinction ratio when using directional couplers. You can see for longer wavelengths the extinction ratio is increased.

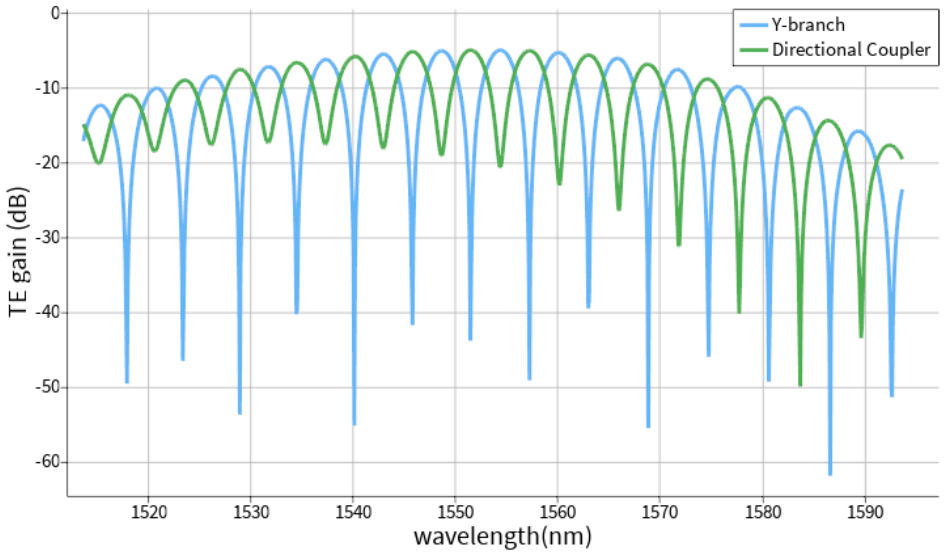

Fig. 21: Transmission of the MZI with Y-branch (blue) and directional coupler (green)

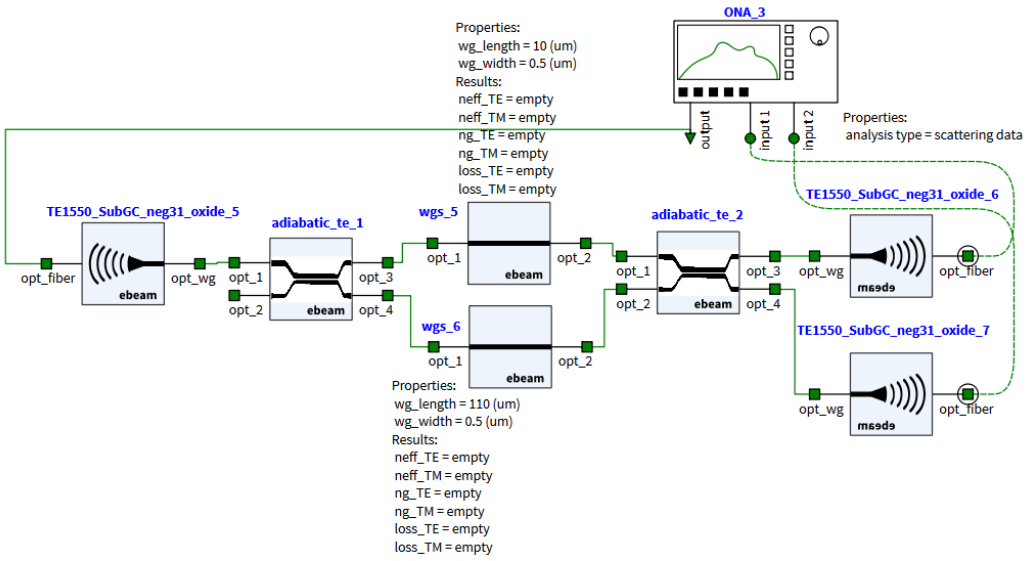

Fig. 22: MZI with adiabatic couplers in INTERCONNECT

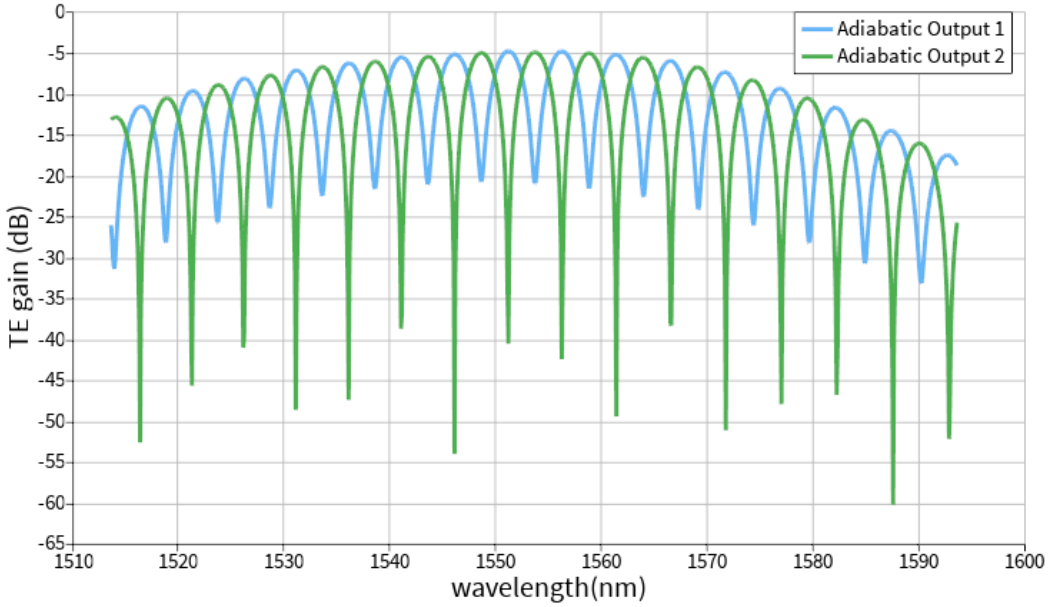

Fig. 23: Transmission of the MZI with adiabatic couplers

4. Layout

The design proposal was developed in KLayout. The draft layout mask is depicted in Figure 24.

A few details were demanded in design, to make possible the future automated testing. The main considered restrictions were the following:

- The TE and TM grating couplers were oriented to the right side, to speed up the tests, avoiding unnecessary chip rotations.
- A 127 µm pitch was fixed, for the input and output gratings, to match with the pitch of the fiber array used in the automated measurements.
- To mitigate the bend losses, all the TE-devices curves have a radius of 5 µm, while TM-devices have curves of 10 µm. As the TM mode has a lower effective index, it is less confined, requiring a higher radius to account for bend losses.

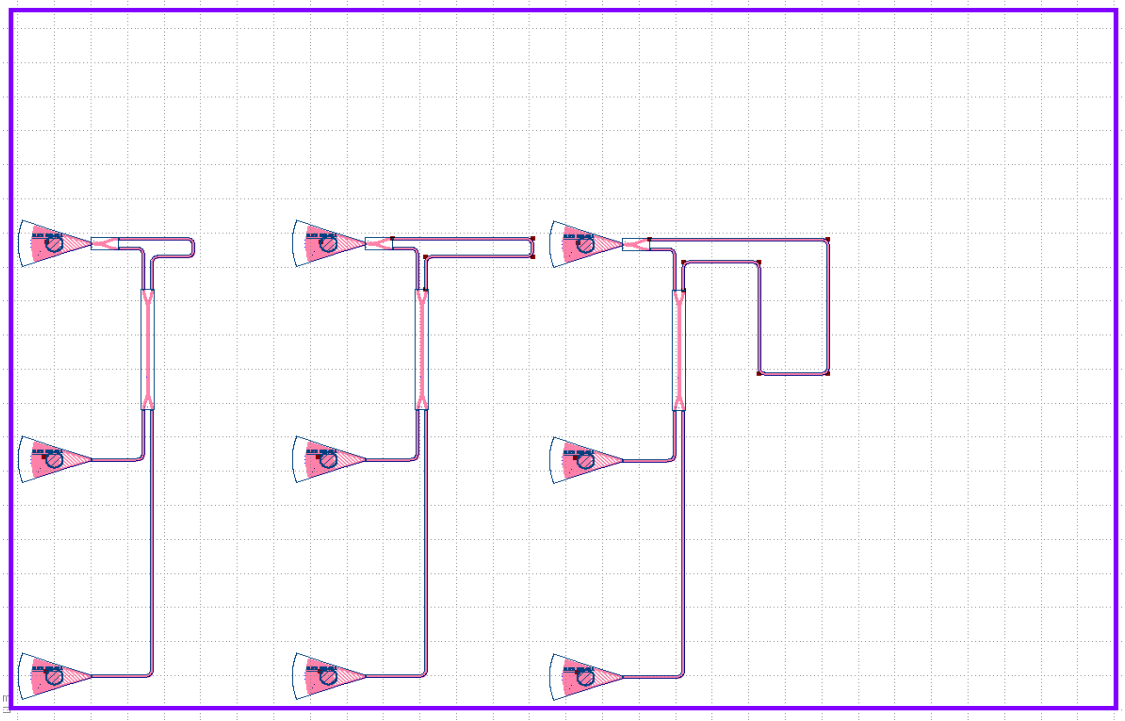

Fig. 24: Initial layout in Klayout

Figures 25-27 shows the INTERCONNECT simulation results of the above layouts.

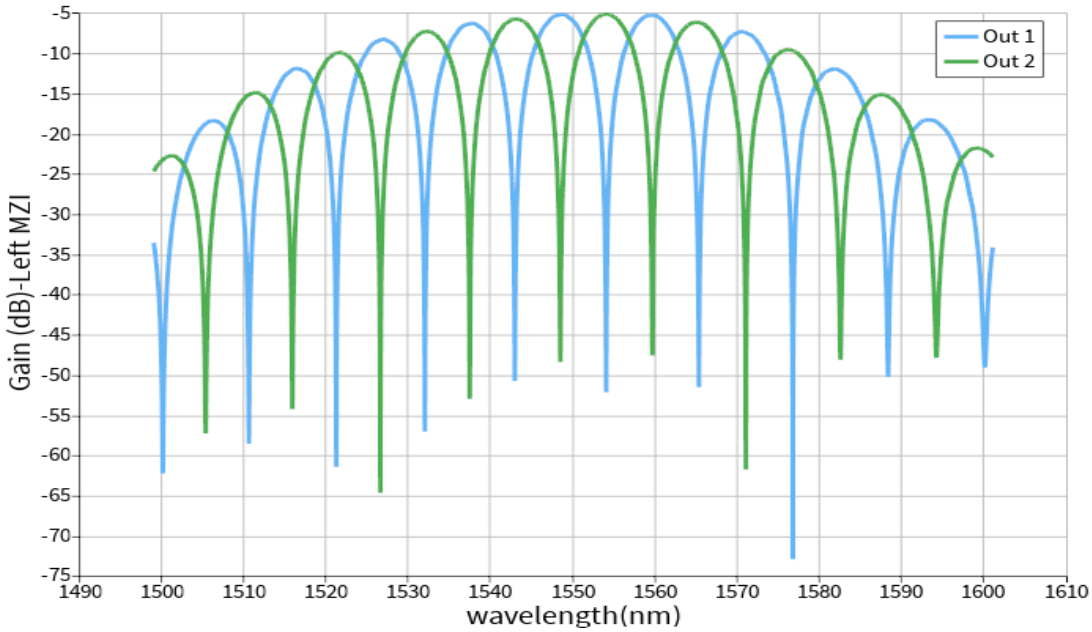

Fig. 25: Transmission result of the left MZI in the layout

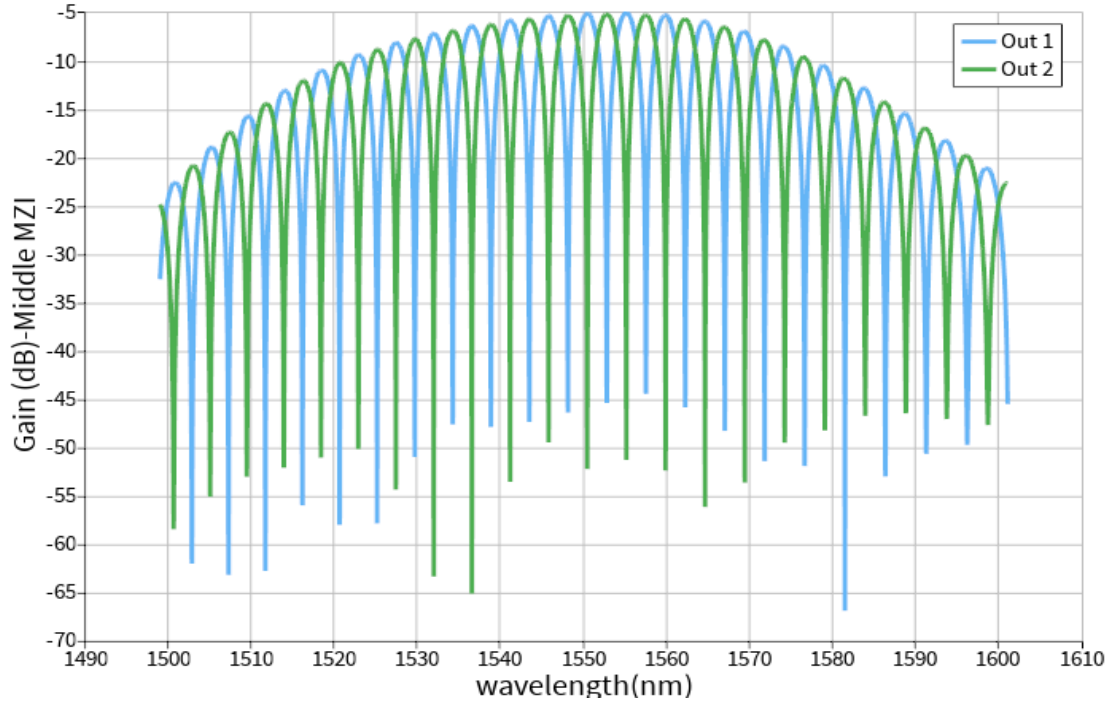

Fig. 26: Transmission result of the middle MZI in the layout

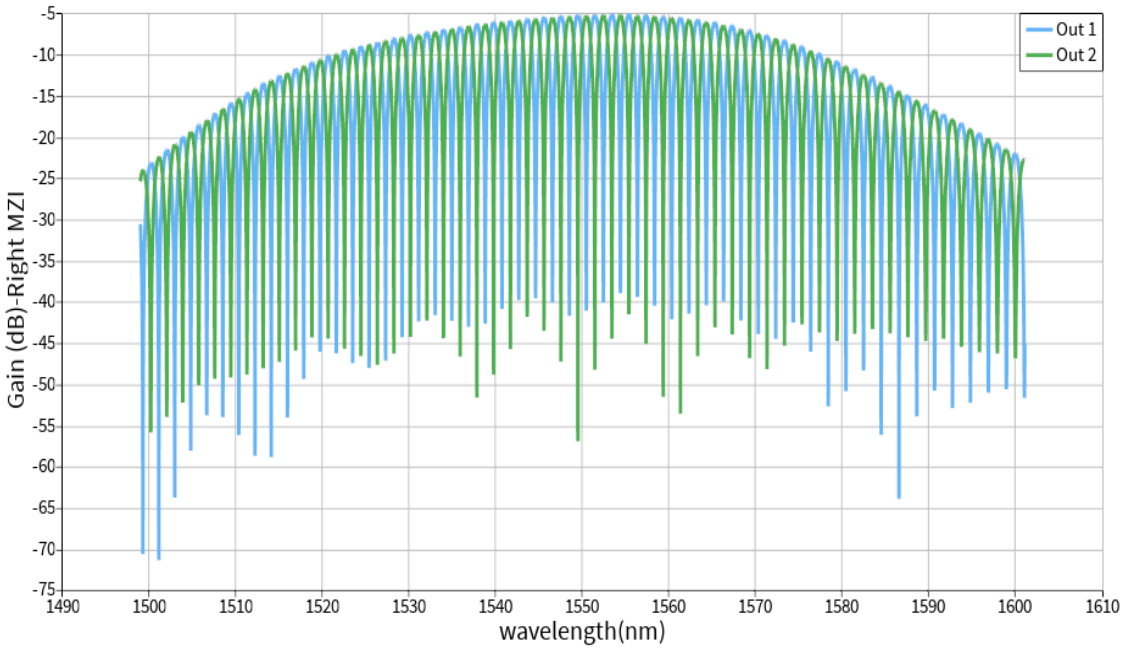

Fig. 27: Transmission result of the right MZI in the layout

As expected, the MZI with higher ΔL has smaller FSR.
We also performed Monte Carlo simulations for the left MZI for 2 wafers each with 2 dies. The Lumerical INTERCONNECT results are shown in figure 28.

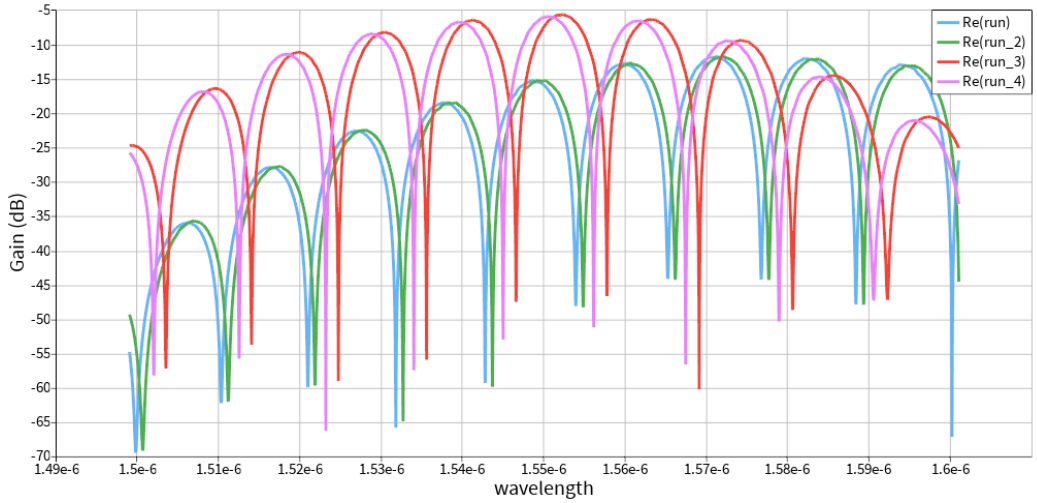

Fig. 28: Monte Carlo simulation results for the left MZI